Morphology of low-temperature homoepitaxial growth on laser-textured Ge(001)

Arvind Raviswaran* and David G. Cahill†
Department of Materials Science and Engineering, and Frederick Seitz Materials Research Laboratory, University of Illinois, Urbana, Illinois 61801, USA
(Received 24 November 2003; published 20 April 2004)

We delineate the growth conditions of temperature, substrate vicinality, and hydrogen termination that produce rough and smooth crystal growth of Ge by molecular beam epitaxy. Ge(001) substrates are modified by laser texturing to produce all azimuths of miscuts θ in the range $0° < \theta < 10°$ within a 4 μm diameter laser dimple. We deposit Ge on these modified substrates over a wide range of growth temperatures $150\,°\mathrm{C} < T < 400\,°\mathrm{C}$, with and without an atomic hydrogen flux of 3×10^{13} cm^{-2} s^{-1}, and characterize the morphologies by atomic-force microscopy. Ridge-shaped growth instabilities dominate the morphology for miscuts toward $\langle 110\rangle$ directions; in regions with miscuts toward $\langle 100\rangle$ the morphology is relatively smooth. Hydrogen flux suppresses the growth-mound instability at small miscuts and reduces the epitaxial critical thickness at large miscuts.

DOI: 10.1103/PhysRevB.69.165313 PACS number(s): 81.10.Aj, 81.15.Aa, 81.15.Kk, 68.55.−a

I. INTRODUCTION

The morphology of crystal growth at low temperatures is often unstable. Asymmetries in the kinetics of adatom attachment at step edges[1–3] or asymmetries in the motion of adatoms past kink sites[4–6] generate a purely kinetic mechanism for roughening of a planar surface. Random nucleation is thought to produce local smoothing[7] and the balance between smoothing on small length scales and roughening on large length scales leads to pattern formation[8] and the appearance of a periodic arrangement of growth mounds during growth on well-oriented low-index crystal surfaces. Growth-mound instabilities have been observed in numerous experiments and computational models;[9–11] thorough reviews of this literature can be found in Refs. 12 and 13.

On surfaces with large miscuts and a high density of steps, we can classify the morphological instabilities into two broad categories: (i) instabilities of the step spacing, usually referred to as "step-bunching" instabilities; and (ii) instabilities of the step morphology, often referred to as step-meandering or step-fingering instabilities. Asymmetries in attachment kinetics—the so-called Ehrlich-Schwoebel barrier—suppress step-bunching instabilities[14] but provide an enabling mechanism for a step-fingering instability.[15] Thus, the morphologies of $(1+1)$-dimensional models of vicinal surfaces are stabilized by an Ehrlich-Schwoebel barrier[7] while realistic vicinal surfaces in $2+1$ dimensions are typically unstable[16–19] and often form ridge-shaped instabilities aligned along the miscut direction. [The step-bunching instabilities observed during growth on vicinal Si(001) are a notable exception.[20,21]]

To provide a more complete set of data for roughening and pattern formation on vicinal surfaces, we have studied homoepitaxial growth on laser-textured Ge(001). Laser texturing[22] provides a simple and clean method for creating a small region of the surface that contains all miscuts and miscut azimuths within $\sim10°$ of the substrate normal. Thus, we can efficiently delineate the miscut dependence of the growth morphology for various film thicknesses $50 < h < 450$ nm and growth temperatures $150\,°\mathrm{C} < T < 450\,°\mathrm{C}$. These large film thicknesses are required because the growth instability of Ge(001) is weak: the Ehrlich-Schwoebel length[7] is comparable to the surface lattice constant[18] and therefore much smaller than the critical terrace size for island nucleation.[7,18,23]

Millimeter-sized concave-shaped substrates prepared by mechanical grinding have been used previously in studies of the equilibrium reconstructions and step spacings of Si surfaces[24–26] and instabilities of the step morphology driven by electric fields.[27] The advantages of our micron-sized dimples created by laser texturing are the experimental convenience and the fact that the entire dimple can be imaged at high resolution using a single scan area of an atomic-force microscope.

II. EXPERIMENTAL DETAILS

Ge(001) wafers with miscut $< 0.1°$ are cleaned by repeated ozone-assisted oxidation and removal of the oxide in water and then textured with individual pulses from a frequency-doubled YAG (yttrium aluminum garnet) laser ($\lambda = 532$ nm) to create smooth laser dimples $\simeq 4$ μm in diameter and 120 nm in depth.[28] Typical parameters of the focused laser spot are a peak fluence of $\simeq 0.6$ J cm^{-2} and a $1/e^2$ radius of $\simeq 5$ μm. The threshold fluence for melting of Ge is 0.14 J cm^{-2}. Samples are In bonded to a Mo sample block and the final oxide layer is removed in the growth chamber by annealing for 30 min at 450 °C.

To produce a clean starting surface for the growth experiments, we deposit a 20 nm thick Ge buffer layer at 330 °C by molecular-beam epitaxy using electron-beam evaporation of Ge.[10,18] The buffer-layer growth temperature and thickness have been optimized to minimize the roughness of low-miscut surfaces while avoiding excessive roughening of vicinal surfaces by step bunching and the formation of high-index facets.[18] The deposition rate is 0.1 nm s^{-1} and the chamber pressure rises to $\approx 2\times10^{-9}$ Torr during Ge deposition. Samples are rotated at 5 rpm to minimize any possible influence of shadowing of the growth flux. After deposition, we immediately turn off the substrate heater to begin cooling

 ©2004 The American Physical Society

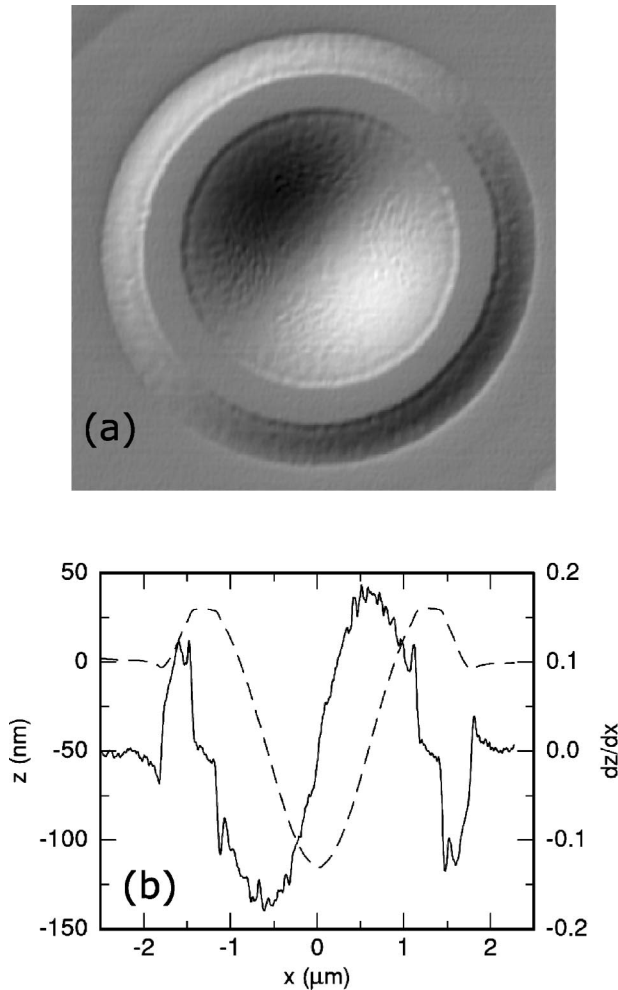

FIG. 1. (a) Atomic-force microscopy (AFM) image of a laser dimple on Ge(001) after growth of a 20 nm thick buffer layer at 330 °C. The gray scale of the image is keyed to the derivative of the surface profile taken along a path from the upper left to lower right of the image. The lateral extent of the image is 4 μm. (b) Analysis of the morphology across the center, from left to right, of the laser dimple shown in (a). The surface height z (dashed line) is plotted vs the left axis; the derivative of this profile dz/dx (solid line) is plotted vs the right axis.

the sample; the cooling rate is $\approx 2\ °\mathrm{C\,sec}^{-1}$. Growth temperatures are measured using an infrared pyrometer operating in the wavelength band $4.8<\lambda<5.2\ \mu$m with a constant emissivity $\epsilon=0.45$ that takes into account the transmissivity of the sapphire viewport.

Images of the surface morphology are acquired using atomic-force microscopy (AFM) in tapping mode after removing the sample from the deposition chamber. An AFM image of a typical starting surface is shown as Fig. 1. Growth of the thin buffer layer at 330 °C does not modify the shape of the laser dimple significantly except for a flattening of the top of the rim that surrounds the bowl-shaped depression at the center of the laser dimple. The inner diameter of this rim is $\approx 2.5\ \mu$m. The miscut $\theta=\arctan(dz/dx)$ varies continuously from $\theta=0$ at the center of the dimple to a maximum of $\theta\simeq 10°$ at a radius of $\approx 0.6\ \mu$m and then decreases to $\theta \simeq 6°$ near the inner diameter of the rim, see Fig. 1(b).

A thermal cracker for hydrogen supplied by Applied Epi is used to generate an atomic-hydrogen flux for experiments on growth on hydrogen-terminated surfaces. The background pressure of H_2 in the chamber is 10^{-6} Torr during the operation of this source. The atomic H flux of $(3\pm1)\times10^{13}\ \mathrm{cm}^{-2}\,\mathrm{s}^{-1}$ was calibrated by measuring the erosion of an amorphous hydrogenated carbon (a-C:H) film at $T=375\ °$C over a period of 48 h: on average, each H incident on the a-C:H film removes 0.02 ± 0.007 C atoms.[22] The change in thickness of the a-C:H film was measured by spectroscopic, variable-angle ellipsometry.

III. RESULTS AND DISCUSSION

Figure 2 displays AFM images of $h=450$ nm thick epitaxial layers at growth temperatures of 200, 250, and 300 °C. At 200 and 250 °C, the singular surfaces surrounding the laser dimple and the top of the rim of the laser dimple show symmetrical growth-mounds in agreement with our earlier work.[10,18] Vicinal surfaces with miscuts toward $\langle 110\rangle$ directions show anisotropic growth ridges aligned along $\langle 110\rangle$ directions.[18] At 300 °C, growth mounds do not form on singular surfaces but low aspect-ratio growth ridges persist in regions of high miscut.

We focus on two surprising results in Fig. 2. First, the growth ridges are always aligned along $\langle 110\rangle$ direction, not the local miscut direction. (If the ridges were always aligned along the local miscut directions, the tops of the ridges would point radially toward the center of the dimple.) Second, growth morphologies are relatively smooth in regions with large miscuts toward the $\langle 100\rangle$ directions. These domains of miscut do not appear to be absolutely stable against roughening: at low temperatures, growth ridges fill most of the area inside the dimple although areas of smooth growth are still visible for miscuts that are well aligned in $\langle 100\rangle$ directions, see in particular the sloped surfaces surrounding the outer edge of the rim in Fig. 2(a). At higher growth temperatures, $T\geqslant 250\ °$C, relatively large domains of smooth growth exist for $h=450$ nm but we have not determined if the smooth surfaces are maintained at significantly greater film thickness.

Statistical measures of the morphologies in seven growth experiments, $150°<T<250\ °$C and $50<h<450$ nm, are summarized in Fig. 3. This analysis is for miscuts near the $\langle 110\rangle$ azimuth where the roughness is largest and the growth ridges are most fully developed. The roughness is only weakly dependent on the magnitude of the miscut for $h<150$ nm but the roughness has a maximum near $\theta=6°$ for $h=450$ nm. In all cases, the lateral separation between growth ridges decreases with increasing miscut for $\theta<3°$ and becomes independent of miscut for $\theta>5°$. The data plotted in Fig. 3 are in quantitative agreement with our previous study of growth on vicinal surfaces with homogeneous miscuts of 6° and 9°.[18]

At the largest film thickness, $h=450$ nm, ridge-shaped instabilities for miscuts in the $\langle 110\rangle$ direction are perceptible at a growth temperature of 350 °C (data not shown) and are completely eliminated only at 400 °C, see Fig. 4. The shape

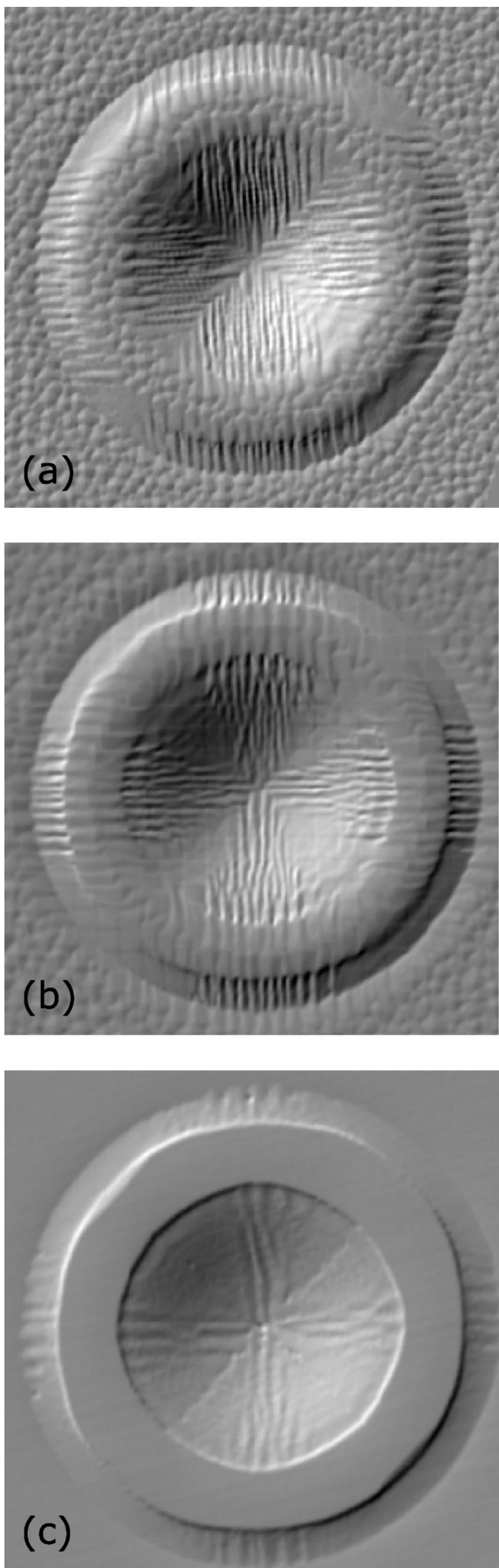

FIG. 2. AFM image of Ge(001) growth at (a) 200 °C; (b) 250 °C; and (c) 300 °C. The film thickness for all three cases is 450 nm. The lateral extent of each image is 4 μm. The gray scale of the image is keyed to the derivative of the surface profile taken along a path from the upper left to lower right of the image. The ⟨110⟩ directions are oriented horizontally and vertically.

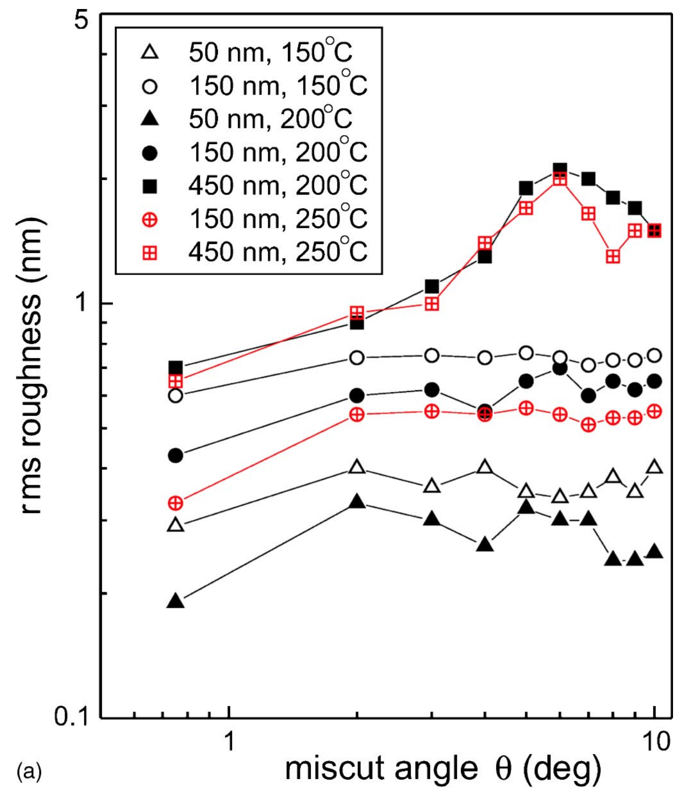

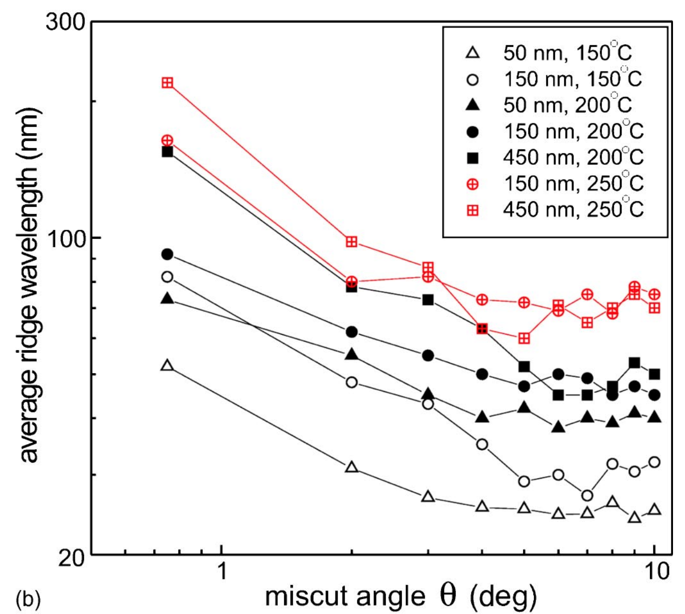

FIG. 3. (Color online) Analysis of the local morphology of regions inside the laser dimple with miscuts toward the ⟨110⟩ directions. (a) rms surface roughness; the amplitude of the periodic structures is approximately $\sqrt{2}$ larger than the rms roughness. The data points plotted at $\theta = 0.75°$ represent an average over miscuts $0° < \theta < 1.5°$. The legend gives the layer thickness and growth temperature; the roughness is a stronger function of film thickness than of growth temperature. (b) Lateral length scale, i.e., the wavelength or periodicity, of the ridge-shaped morphologies. The lateral scale is a stronger function of growth temperature than of film thickness.

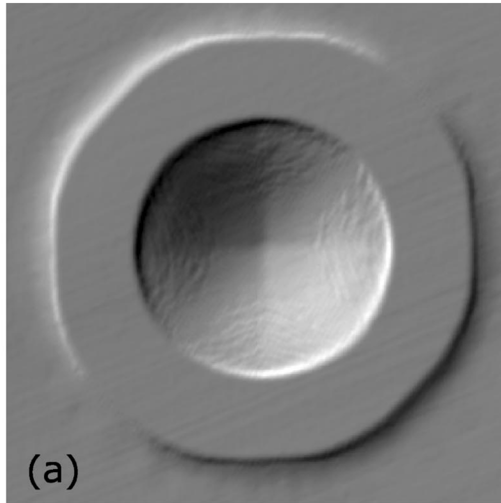

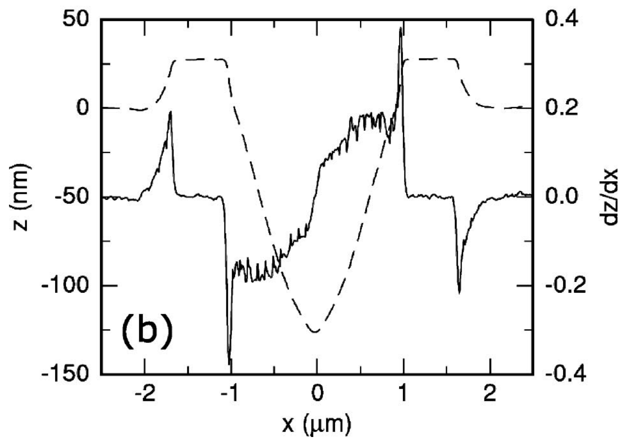

FIG. 4. AFM image of Ge(001) growth at 400 °C. The film thickness is 450 nm; the lateral extent of the image is 4 μm. (b) Analysis of the morphology across center, from left to right, of the laser dimple shown in (a). The surface height z (dashed line) is plotted vs the left axis; the derivative of this profile dz/dx (solid line) is plotted vs the right axis.

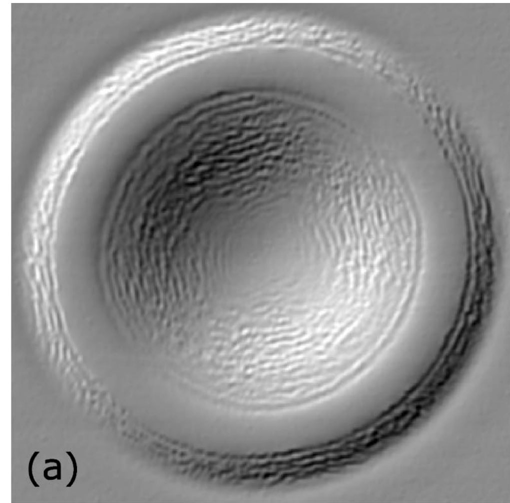

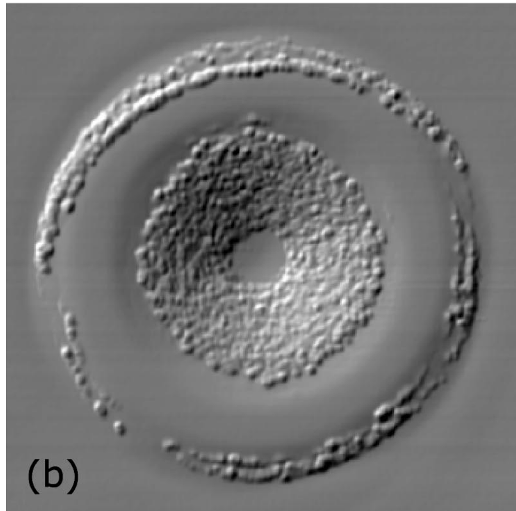

FIG. 5. Atomic-force microscopy image Ge(001) growth accompanied by an atomic-hydrogen flux of $3\times10^{13}\,\mathrm{s}^{-1}$ at growth temperatures of (a) 250 °C and (b) 200 °C. The film thicknesses are 285 and 450 nm, respectively.

of the laser dimple is strongly modified by epitaxial growth at this relatively high temperature: the flat rim is now 0.6 μm wide and surrounded by steep sidewalls with slopes as large as 20°. Within the laser dimple, step bunching with a periodicity of $\approx$90 nm is pronounced.

We have also investigated the effects of an atomic hydrogen flux on the growth morphology. After growth of the buffer layer, we reduce the temperature of the sample to the desired temperature, turn on an atomic-hydrogen flux of $3\times10^{13}\,\mathrm{cm}^{-2}\,\mathrm{s}^{-1}$, and wait 10 min before initiating deposition of Ge. The H flux is maintained throughout the duration of the growth.

Results of these experiments are shown in Fig. 5. Unfortunately, we do not have instrumentation in our analysis chambers capable of measuring the surface coverage of H. By analogy with previous studies of Si growth,[29] we conclude that H will continuously segregate to the Ge surface at the temperatures we have investigated, $150° < T < 250\,°\mathrm{C}$. The steady-state coverage of H is more difficult to ascertain. At 150 °C, the dihydride phase is stable and at 250 °C the dihydride phase is unstable on time scales of $\approx$1 min.[30] Thus, we assume that the steady-state H coverage in a flux of $3\times10^{13}\,\mathrm{cm}^{-2}\,\mathrm{s}^{-1}$ will be >1 at 150 °C and will be $\simeq 1$ at 250 °C.

A H flux is known to reduce the critical thickness h_{epi} for epitaxial growth of Si;[29,31] i.e., epitaxial growth breaks down for films of thickness $h > h_{epi}$ with the formation of polycrystalline or amorphous layers. For Ge(001), $h_{epi} \simeq 1$ μm at $T = 150\,°\mathrm{C}$ and h_{epi} diverges as T approaches 170 °C.[32] We have observed that a 50 nm Ge film deposited at 150 °C in the presence of a H flux is amorphous for all miscuts (data not shown), in agreement with the conclusion of Ref. 29 that epitaxial growth is strongly inhibited on dihydride-terminated surfaces. Growth at 250 °C is epitaxial for all thickness and miscuts, see Fig. 5. Growth at 200 °C is an intermediate case: on low-miscut surfaces $h_{epi} > 450$ nm but for miscuts $\theta > 5°$, $150 < h_{epi} < 450$ nm. The mottled rough-

ness in Fig. 5(b) is caused by the breakdown in epitaxial growth for $\theta > 5°$.

Figure 5 also shows that the growth-mound instability of epitaxial growth on low-miscut surfaces is completely suppressed by a H flux at 200 °C and 250 °C. On vicinal surfaces at 250 °C, hydrogen coverage removes the growth-ridge instability and induces a step-bunching instability that is essentially independent of the azimuth of the miscut.

IV. CONCLUSIONS

We find that growth ridges on Ge(001), when present, are aligned along $\langle 110\rangle$ directions, not along the local miscut direction; and growth ridges are inhibited in regions with large miscuts in the $\langle 100\rangle$ directions. Our experiments alone, however, cannot pinpoint the cause of this anisotropy. Anisotropy of the step stiffness may be playing a role in controlling the growth rate and alignment of the growth ridges but is unclear to us how a thermodynamic quantity such as step stiffness can apply in the low-temperature limit when the step mobility is negligible. In this sense, our experiments are very different from the changes in step morphology created, for example, by heavy B doping of the Si(001) surface[33] or instabilities in step morphologies that are driven by electric fields.[27,34]

One possible explanation of the alignment of the growth-ridges along $\langle 110\rangle$ directions is that the effective asymmetry in the kinetics of adatom attachment—i.e., the effective Ehrlich-Schoebel length l_{ES}—is stronger in $\langle 110\rangle$ directions than in $\langle 100\rangle$ directions. A continuum description of the vector diffusion-bias current[7] as a function of the substrate miscut and miscut azimuth would be useful in testing that assumption.

Smooth growth is enhanced by miscuts in the $\langle 100\rangle$ directions but, if patterned morphologies are desired, the aspect ratio of the growth ridges can be optimized by choosing an intermediate growth temperature $T = 200$ °C and miscut $\theta = 6°$ in the $\langle 110\rangle$ direction. For thick layers, the amplitude-to-wavelength ratio of the growth ridges approaches ≈ 0.1

Growth-mound and growth-ridge instabilities are suppressed by hydrogen coverage. This observation is not unexpected since surface diffusion is required to produce the instabilities driven by diffusion-bias currents and hydrogen adsorption is known to dramatically reduce the surface mobility of adatoms.[35] Therefore, large amplitude, long-wavelength growth instabilities can be suppressed at the cost of increased atomic-scale roughness created by shot noise of the deposition flux.

ACKNOWLEDGMENTS

This material is based upon work supported by the U.S. Department of Energy, Division of Materials Sciences under Grant No. DEFG02-91ER45439, through the Frederick Seitz Materials Research Laboratory at the University of Illinois at Urbana-Champaign. Research for this publication was carried out in the Center for Microanalysis of Materials, University of Illinois at Urbana-Champaign, which is partially supported by the U.S. Department of Energy under Grant No. DEFG02-91-ER45439.

*Present address: Cypress Semiconductor Inc., 2401 E. 86th St., Bloomington, MN 55245.

†Electronic address: d-cahill@uiuc.edu

[1] G. Ehrlich and F.G. Hudda, J. Chem. Phys. **44**, 1039 (1966).

[2] J. Villain, J. Phys. I **1**, 19 (1991).

[3] M.D. Johnson, C. Orme, A.W. Hunt, D. Graff, J. Sudijono, L.M. Sander, and B.G. Orr, Phys. Rev. Lett. **72**, 116 (1994).

[4] O. Pierre-Louis, M.R. D'Orsogna, and T.L. Einstein, Phys. Rev. Lett. **82**, 3661 (1999).

[5] M.V. Ramana Murty and B.H. Cooper, Phys. Rev. Lett. **83**, 352 (1999).

[6] P.P. Chatraphorn, Z. Toroczkai, and S. Das Sarma, Phys. Rev. B **64**, 205407 (2001).

[7] P. Politi and J. Villain, Phys. Rev. B **54**, 5114 (1996).

[8] D.G. Cahill, J. Vac. Sci. Technol. A **21**, S110 (2003).

[9] J.A. Stroscio, D.T. Pierce, M.D. Stiles, A. Zangwill, and L.M. Sander, Phys. Rev. Lett. **75**, 4246 (1995).

[10] J.E. Van Nostrand, S.J. Chey, M.-A. Hasan, D.G. Cahill, and J.E. Greene, Phys. Rev. Lett. **74**, 1127 (1995).

[11] M. Kalff, P. Smilauer, G. Comsa, and T. Michely, Surf. Sci. **426**, L447 (1999).

[12] P. Politi, G. Grenet, A. Marty, A. Ponchet, and J. Villain, Phys. Rep. **324**, 271 (2000).

[13] T. Michely and J. Krug, *Islands, Mounds, and Atoms, Patterns and Processes in Crystal Growth Far from Equilibrium*, Spinger Series in Surface Sciences Vol. 42 (Springer-Verlag, Berlin, 2004).

[14] R.L. Schwoebel and E.J. Shipsey, J. Appl. Phys. **37**, 3682 (1966).

[15] G.S. Bales and A. Zangwill, Phys. Rev. B **41**, 5500 (1990).

[16] N.E. Lee, D.G. Cahill, and J.E. Greene, Phys. Rev. B **53**, 7876 (1996).

[17] M. Rost, P. Smilauer, and J. Krug, Surf. Sci. **369**, 393 (1996).

[18] J.E. Van Nostrand, S.J. Chey, and D.G. Cahill, Phys. Rev. B **57**, 12 536 (1998).

[19] H. Emmerich, Phys. Rev. B **65**, 233406 (2002).

[20] C. Schelling, G. Springholz, and F. Schäffler, Phys. Rev. Lett. **83**, 995 (1999).

[21] J. Mysliveček, C. Schelling, F. Schäffler, G. Springholz, P. Šmilauer, J. Krug, and B. Voigtländer, Surf. Sci. **520**, 193 (2002).

[22] T. Schwarz-Selinger, A. von Keudell, and W. Jacob, J. Vac. Sci. Technol. A **18**, 995 (2000).

[23] B.W. Karr, D.G. Cahill, I. Petrov, and J.E. Greene, Phys. Rev. B **61**, 16 137 (2000).

[24] M. Hanbücken, B. Röttger, and H. Neddermeyer, Appl. Surf. Sci. **164**, 91 (2000).

[25] X. Tong and P.A. Bennett, Phys. Rev. Lett. **67**, 101 (1991).

[26] M. Hanbücken, B. Röttger, and H. Neddermeyer, Surf. Sci. **331-333**, 1028 (1995).

[27] J.-F. Nielsen, M.S. Pettersen, and J.P. Pelz, Surf. Sci. **480**, 84 (2001).

[28] T. Schwarz-Selinger, D.G. Cahill, S.-C. Chen, S.-J. Moon, and C.P. Grigoropoulos, Phys. Rev. B **64**, 155323 (2001).

[29] M. Copel and R.M. Tromp, Phys. Rev. Lett. **72**, 1236 (1994).

[30] L. Papagno, X.Y. Shen, J. Anderson, G. Schirripa Spagnolo, and

G.J. Lapeyre, Phys. Rev. B **34**, 7188 (1986).
[31] D.P. Adams, S.M. Yalisove, and D.J. Eaglesham, Appl. Phys. Lett. **63**, 3571 (1993).
[32] K.A. Bratland, Y.L. Foo, J.A.N.T. Soares, T. Spila, P. Desjardins, and J.E. Greene, Phys. Rev. B **67**, 125322 (2003).
[33] D.E. Jones, J.P. Pelz, Y. Hong, E. Bauer, and I.S.T. Tsong, Phys. Rev. Lett. **77**, 330 (1996).
[34] K. Yagi, H. Minoda, and M. Degawa, Surf. Sci. Rep. **43**, 45 (2001).
[35] M. Okada, A. Muto, H. Ikeda, S. Zaima, and Y. Yasuda, J. Cryst. Growth **188**, 119 (1998).